CrossMark

Evaluation of major heat waves' mechanisms in EURO-CORDEX RCMs over Central Europe

Ondřej Lhotka[1,2] · Jan Kyselý[1,3] · Eva Plavcová[1]

Abstract The main aim of the study is to evaluate the capability of EURO-CORDEX regional climate models (RCMs) to simulate major heat waves in Central Europe and their associated meteorological factors. Three reference major heat waves (1994, 2006, and 2015) were identified in the E-OBS gridded data set, based on their temperature characteristics, length and spatial extent. Atmospheric circulation, precipitation, net shortwave radiation, and evaporative fraction anomalies during these events were assessed using the ERA-Interim reanalysis. The analogous major heat waves and their links to the aforementioned factors were analysed in an ensemble of EURO-CORDEX RCMs driven by various global climate models in the 1970–2016 period. All three reference major heat waves were associated with favourable circulation conditions, precipitation deficit, reduced evaporative fraction and increased net shortwave radiation. This joint contribution of large-scale circulation and land–atmosphere interactions is simulated with difficulties in majority of the RCMs, which affects the magnitude of modelled major heat waves. In some cases, the seemingly good reproduction of major heat waves' magnitude is erroneously achieved through extremely favourable circulation conditions compensated by a substantial surplus of soil moisture or vice versa. These findings point to different driving mechanisms of major heat waves in some RCMs compared to observations, which should be taken into account when analysing and interpreting future projections of these events.

1 Introduction

In the past two decades, Europe experienced several extraordinary heat waves with substantial consequences for ecosystems and society. The 2003 and 2010 'mega heat waves' (Barriopedro et al. 2011) were associated with tens of thousands excess deaths (Robine et al. 2008; Shaposhnikov et al. 2014), decreased plant productivity and crop failures (Bastos et al. 2014), forest fires (Konovalov et al. 2011), record-breaking loss of Alpine glaciers' mass (De Bono et al. 2004), and other impacts.

Such severe heat waves are one of the main concerns with respect to the ongoing climate change (Kirtman et al. 2013). Beniston (2004) concluded that the summer of 2003 bears a close resemblance to what many climate models simulate for summers in the late twenty-first century. The frequency of heat waves over Central Europe is projected to be roughly doubled in the 2020–2049 period compared to historical climate (1970–1999), and this increment was found under all Representative Concentration Pathways (RCP) scenarios. By contrast, in the late twenty-first century, the increase of the heat wave frequency (by a factor of 2–5) is scenario-dependent (Lhotka et al. 2017). These changes are expected

✉ Ondřej Lhotka
ondrej.lhotka@ufa.cas.cz

1 Institute of Atmospheric Physics, Czech Academy of Sciences, Prague, Czech Republic

2 Global Change Research Institute, Czech Academy of Sciences, Brno, Czech Republic

3 Faculty of Environmental Sciences, Czech University of Life Sciences, Prague, Czech Republic

to be primarily driven by a shift of the temperature distribution (Ballester et al. 2010; Lau and Nath 2014), but Fischer and Schär (2010) also identified larger variance of summer temperature distribution in a possible future climate, and Lhotka et al. (2017) pointed out increased temporal autocorrelation of daily maximum temperature, suggesting more persistent heat waves.

Before analysing projections for a possible future climate, model simulations have to be evaluated against historical data. Kotlarski et al. (2014) evaluated regional climate model (RCM) simulations from the EURO-CORDEX project (COordinated Regional climate Downscaling EXperiment, Jacob et al. 2014) that were driven by the ERA-Interim reanalysis (Dee et al. 2011). The majority of RCMs overestimated summertime temperature over Southern and Eastern Europe, while underestimation was found in Scandinavia and the British Isles. The capability of reanalysis-driven EURO-CORDEX RCMs to simulate heat waves over Europe was investigated by Vautard et al. (2013), who concluded that models had too-persistent and too-intense heat waves, even though the influence of the temperature bias was removed. The enhanced severity of heat waves in the ENSEMBLES RCMs (van der Linden and Mitchell 2009) driven by reanalysis was reported by Lhotka and Kyselý (2015b), who found a connection between the magnitude of heat waves and precipitation during and before these events. Inasmuch as most precipitation during heat waves is of convective origin (Stéfanon et al. 2014), this result is in accordance with Vautard et al. (2013), who discussed a possible connection between exaggerated land–atmosphere feedbacks and overestimated heat wave severity in the RCMs.

Soil moisture is an important variable in these land–atmosphere interactions, because it controls the partitioning of available energy between sensible and latent heat fluxes at the surface (Berg et al. 2014). The link between reduced soil moisture and amplified summer temperature in an RCM was shown, for example, by Jaeger and Seneviratne (2011). Using also a reanalysis-driven RCM, Stéfanon et al. (2014) found different relationships between a soil moisture deficit and severity of heat waves over lowlands, mountains, and coastal areas. In lowlands, a reduction of soil moisture led to less evapotranspiration and higher sensible heat flux, which consequently caused a drier atmosphere and therefore less clouds and precipitation. Stéfanon et al. (2014) estimated that this process contributed as much as 20% of the temperature anomaly in Eastern France and Western Germany during heat waves.

Using reanalysis-driven RCMs from the ENSEMBLES project, Stegehuis et al. (2013) demonstrated that most models in their study exhibited overestimated drying during warm seasons, leading to the establishment of a soil moisture-limited regime across Europe in summer. Inasmuch as an analogously large soil moisture deficit was found only over the Iberian Peninsula in observed data from the FLUXNET network (the global network of micrometeorological tower sites, Baldocchi et al. 2001), this RCMs' deficiency may contribute to overestimation of the frequency and severity of heat waves. The important role of RCMs' land surface scheme for a proper simulation of temperature and surface fluxes was also shown by Davin et al. (2016), who demonstrated that the COSMO-CLM RCM with more advanced representation of land processes outperforms EURO-CORDEX RCMs in many characteristics.

An important factor conducive to heat waves is atmospheric circulation. Severe European heat waves are triggered by a combination of radiative heating due to clear-sky conditions and southerly to easterly advection of warm air masses (e.g. Della-Marta et al. 2007; Kyselý 2008). This favourable setting is especially prolonged during atmospheric blocking episodes (e.g. Schubert et al. 2014). Plavcová and Kyselý (2016) demonstrated that RCMs driven by reanalysis simulate atmospheric circulation during heat waves reasonably well, which is related to the fact that the large-scale flow in RCMs is primarily given by lateral boundary conditions (Plavcová and Kyselý 2012). RCMs seem to be capable, however, of modifying atmospheric circulation through processes inside their domains. For example, Haarsma et al. (2009) showed that an inaccurate simulation of soil moisture regime over Southern Europe may lead to the development of thermal low and consequent easterly advection to Central Europe, with implication for heat waves' severity.

Due to these model deficiencies, it is important to understand whether heat waves in models occur for the same reasons that they do in nature (Fischer 2014). In this study, we analysed the severity of past heat waves in the 1950–2016 period and identified three 'major heat waves' in 1994, 2006, and 2015 that were used as analogues for RCM simulations. Anomalies in atmospheric circulation, precipitation, and surface fluxes are assessed for the observed major heat waves and compared with those simulated by RCMs from the EURO-CORDEX project in the 1970–2016 period. The study is performed over Central Europe, which was recently affected by pronounced heat and drought in summer 2015 (Hoy et al. 2016) and heat waves during this summer were exceptional also at the continental scale (Russo et al. 2015). In contrast to previous studies, the RCMs are driven by global climate models (GCMs) in order to evaluate RCM×GCM combinations that can be used for future projections and to analyse the sources of biases in simulating severe temperature events.

2 Data and methods

2.1 Regional climate model simulations

14 regional climate model (RCM) simulations driven by global climate models (GCMs) were taken from the

EURO-CORDEX project (Jacob et al. 2014) and are listed in Table 1. All RCMs use the 0.11° rotated grid but were recalculated to the 0.22° grid through averaging four respective grid points in order to allow a direct comparison with the E-OBS data set. An analogous procedure was applied by Kotlarski et al. (2014) when comparing the performance of EURO-CORDEX and ENSEMBLES models driven by reanalyses. We employed all available RCM × GCM combinations from the Earth System Grid Federation (ESGF) data node that use the 0.11° rotated grid. Most simulations start in 1950 or 1951 (except for simulations from SMHI, which start in 1970), and they all use historical forcing until 2005. The RCP 4.5 scenario runs (Thomson et al. 2011) were selected for the most recent 2006–2016 period (note that differences between individual scenarios are small in this early period).

2.2 Meteorological variables

Observed heat waves were analysed using daily maximum temperature (Tmax) from the E-OBS 14.0 gridded data set (Haylock et al. 2008). This data set is available from 1950 to the present and has the 0.22° rotated grid, which is the same as the recalculated grid in the EURO-CORDEX RCMs. Besides Tmax, daily precipitation was also taken from this data set. Sea level pressure (SLP), 500 hPa geopotential height (Z500, both at 12 UTC), and surface radiation and energy fluxes (daily means from hourly values) were taken from the ERA-Interim reanalysis (0.25° grid), which is available from 1979 and is regularly updated (Dee et al. 2011). Analogous variables were taken from the RCM simulations, which are analysed for the overlapping 1970–2016 period on a daily basis (Online Resource 1).

2.3 Area of interest

Relationships between major heat waves and the meteorological factors were analysed over Central Europe (Fig. 1a). This region exhibits relatively homogeneous climate and contains 40 × 26 grid points in the 0.22° rotated grid. The area of interest was slightly different when analysing surface radiation and energy fluxes due to a different geographical projection in the ERA-Interim data set.

2.4 Definition of heat waves

The definition of heat waves was analogous to that used in Lhotka and Kyselý (2015a) and was based on positive deviations from the 90% quantile of the summer (June–August, JJA) Tmax distribution, which was calculated for the 1981–2010 reference period. For each day between May 1 and September 30, differences between actual Tmax and the 90% quantile were calculated for every grid point (1,040). The Tmax deviations were then averaged over the grid points and if a resulting number was positive, the given day was considered a hot day. Subsequently, a heat wave occurs if at least three consecutive hot days occur. The extended May–September period was chosen because the warming climate provides a larger potential for early or late heat waves (e.g. the September 2015 heat wave, Hoy et al. 2016). Note that the 90% quantile is still calculated for the summer (JJA) period only.

This definition of heat waves was also applied for RCMs, where the 90% quantiles were calculated separately for each simulation in order to remove the influence of the Tmax bias. This approach is suitable when focusing on the behaviour of the right tail of the Tmax distribution and the spatial and temporal structure of daily temperatures (which are essential for

Table 1 Regional climate models (RCMs) driven by global climate models (GCMs) from the EURO-CORDEX project used in this study

Institute	Acronym	RCM	GCM
Climate Limited-area Modelling Community	CLM	CCLM	CNRM
			HadGEM
			ICHEC
			MPI
Danish Meteorological Institute	DMI	HIRHAM	ICHEC
Institute Pierre Simon Laplace	IPSL	WRF	IPSL
Royal Netherlands Meteorological Institute	KNMI	RACMO	HadGEM
			ICHEC
Max Planck Institute for Meteorology	MPI	REMO	MPI
Swedish Meteorological and Hydrological Institute	SMHI	RCA	CNRM
			HadGEM
			ICHEC
			IPSL
			MPI

All RCMs have the 0.11° rotated grid

Fig. 1 **a** Definition of Central Europe (*black dashed polygon*), with *colour shading* representing the 90% quantile of summer daily maximum temperature (calculated for the 1981–2010 period); **b** points used for calculation of circulation indices (*black numbered dots*) and summer daily maximum temperature standard deviation (*colour shading*, 1981–2010)
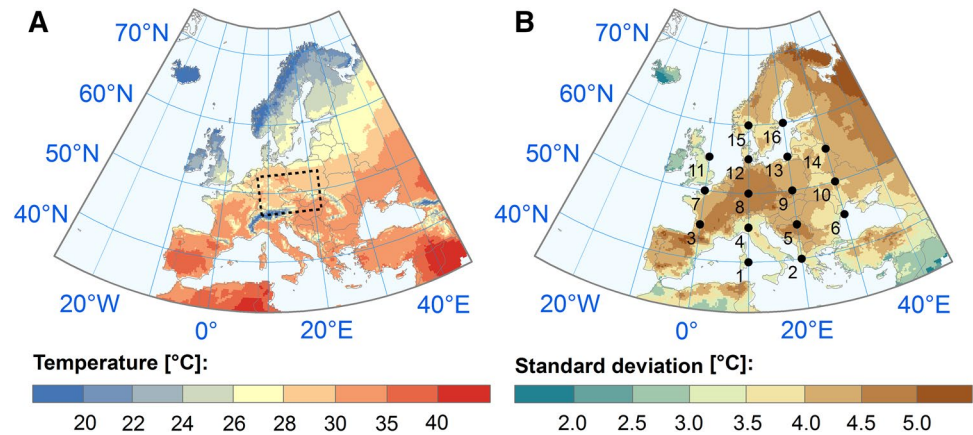
heat waves) rather than on the Tmax bias itself. The overall magnitude of heat waves is assessed through the extremity index (Lhotka and Kyselý 2015a), calculated as the sum of positive Tmax anomalies from the 90% quantile during all days when a heat wave persists (scaled by the number of grid points in Central Europe, i.e. 1,040). This index captures joint effects of the temperature anomaly, length, and spatial extent of heat waves, and 'major heat waves' are defined based on its value of at least 25 °C (see Sect. 3).

2.5 Calculation of circulation indices

Circulation indices were derived from daily gridded SLP data at the 16 grid points shown in Fig. 1b (Jenkinson and Collison 1977; Blenkinsop et al. 2009; Plavcová and Kyselý 2012). In RCMs, SLP values were obtained using an inverse distance-weighted mean of four grid points adjacent to given coordinates, because RCMs do not use a latitude-longitude grid. The western flow component (w) is defined as a pressure gradient between 45°N and 55°N and it is calculated using the formula

$$w = 0.5 \times (p4 + p5) - 0.5 \times (p12 + p13)$$

where p(X) is a SLP in a given grid point (Fig. 1b). The southern flow component (s) is the gradient between 10°E and 20°E, given by the formula

$$s = \frac{1}{\cos\left(\varphi \times \frac{\pi}{180}\right)} \times [0.25 \times (p13 + 2 \times p9 + p5) - 0.25 \times (p12 + 2 \times p8 + p4)]$$

where φ represents the latitude of the centre (50°N) in degrees and p(X) is a SLP in a given grid point, analogously to the western flow component. The total vorticity (vort) is the sum of its zonal (zw) and meridional (zs) components and reflects the rotation of an air mass. It is calculated using the formulas

$$zw = \frac{\sin\left(\varphi \times \frac{\pi}{180}\right)}{\sin\left[(\varphi - 5)\right] \times \frac{\pi}{180}} \times [0.5 \times (p1 + p2) - 0.5 \times (p8 + p9)]$$
$$- \frac{\sin\left(\varphi \times \frac{\pi}{180}\right)}{\sin\left[(\varphi - 5)\right] \times \frac{\pi}{180}} \times [0.5 \times (p8 + p9 - 0.5 \times (p8 + p9)]$$

$$zs = \frac{1}{2 \times \left(\cos\left(\frac{\pi}{180}\right)\right)^2} \times [0.5 \times (p14 + p2 \times p10 + p6)]$$
$$- 0.25 \times (p12 + 2 \times p5 + p4) + 0.25$$
$$\times (p11 + 2 \times p7 + p3)]$$

$$vort = zw + zs$$

where φ represents the latitude of the centre (50°N) in degrees and p(X) is a SLP in a given grid point. Positive (negative) values indicate cyclonic (anticyclonic) conditions.

2.6 Links between major heat waves and meteorological factors

At first, precipitation, net solar radiation, and evaporative fraction from both observed and modelled data were averaged over Central Europe (Fig. 1a) in order to obtain regionally-averaged daily values. Precipitation deficits were calculated for the period during and prior to the major heat waves. The last day of a major heat wave was omitted, because these events are usually terminated by the passage of a cold front, which often brings a large amount of rainfall. Preceding precipitation deficits were assessed for 30-day periods prior to major heat waves. The sum of precipitation during a given period was compared to the 1981–2010 daily-based climatology (calculated for JJA) and expressed as a percentage.

For periods during major heat waves, the daily average of net solar radiation (difference between incoming shortwave radiation at the surface and reflected shortwave radiation) was calculated and expressed in watts per square meter. The amount of soil moisture during major heat waves was assessed indirectly through evaporative fraction, which is the ratio between latent heat flux and the sum of latent and sensible heat fluxes. Note that soil moisture cannot be compared directly between RCMs and the ERA-Interim reanalysis due to different thickness of soil layers (Dee et al. 2011; Kotlarski et al. 2014). Analogously to precipitation, net solar radiation and evaporative fraction during heat waves were compared to the 1981–2010 daily-based climatology and expressed as a percentage.

Changes in atmospheric circulation during major heat waves were assessed through composite maps of SLP and 500 hPa geopotential height and by analysing differences in western and southern flow components and vorticity against their 1981–2010 daily-based climatology. All these characteristics were calculated for individual major heat waves (both observed and simulated) and averaged thereafter.

3 Observed major heat waves and related meteorological factors

In Central Europe, the summer of 2015 was the most distinctive over the 1950–2016 period, according to the seasonal number of hot days and the sum of the heat wave extremity index (Fig. 2). Since 2010, each summer was marked by at least one heat wave and two of the three most extreme summers (according to the seasonal sums of the extremity index) occurred during this 7-year long period.

In 1950–2016, 41 individual heat waves were found (Online Resource 2). Their length ranged from 3 days (by

definition) to 16 days and their extremity index varied from 2.7 to 41.5 °C. The selection of 'major heat waves' was based on the distribution of extremity index, which represents joint effects of temperature, length and spatial extent of heat waves (cf. Section 2.4). A large majority of heat waves have an extremity index lower than 20 °C (Fig. 3), and the three most severe heat waves (in 1994, 2015, and 2006) according to the extremity index are also the longest ones (16, 11, and 13 days, respectively). Therefore, a major heat wave is defined as an event with extremity index ≥25 °C, in order to capture the natural break in the distribution of this characteristic (Fig. 3). Different values were also tested but usage of higher thresholds led to a very small sample size (several RCMs had no major heat wave), while lower thresholds resulted in a presence of relatively short events with very high temperature anomalies that do not share much similarity with persistent heat waves (1994, 2006, and 2015). A sensitivity analysis shows, however, that the main conclusions are little affected by the particular setting of the threshold used to delimit major heat waves.

The 1994 major heat wave (Fig. 4, left column) persisted for 16 days between Jul 22 – Aug 6 and the largest sums of temperature anomalies were observed in the northeastern part of Central Europe, Poland and Baltic
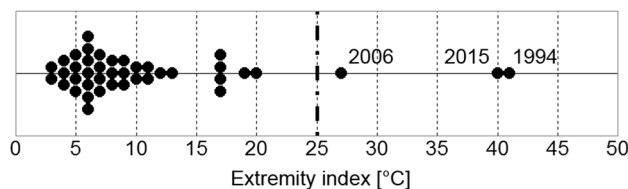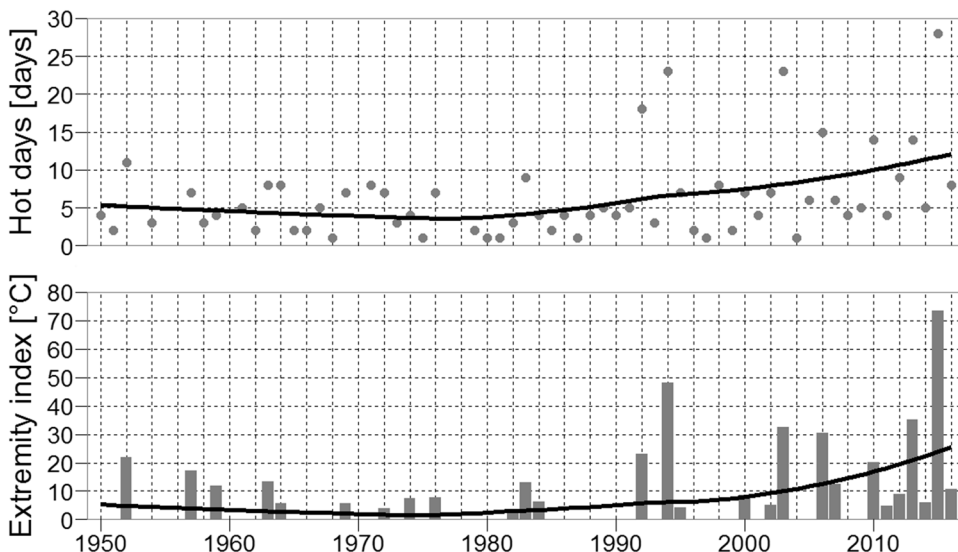

Fig. 3 Dot plots of extremity indices for individual heat waves in E-OBS in the 1950–2016 period

Fig. 2 Time series of the seasonal number of hot days (*dots*) over Central Europe and the sum of the heat wave extremity index (*bars*) in the E-OBS data set for the 1950–2016 period. Solid lines represent the locally weighted scatter plot smoothing (LOESS) *filter curves*

countries. Positive SLP anomalies were located mainly over Fennoscandia and the Baltic region during this event (Fig. 4, middle row). This anticyclone was associated with an elevated Z500 (roughly by up to 150 m), which was a part of a mid-troposphere pattern resembling a so-called 'Rossby wave train' (Fig. 4, bottom row). An Ω blocking pattern is related to this sequence of negative and positive Z500 anomalies that led to reduced zonal flow and advection of warm air masses to Central Europe.

The 2006 major heat wave (Fig. 4, middle column) occurred during the Jul 18 – Jul 28 period and it was the shortest (11 days) of the three events. Compared to the 1994 major heat wave, positive temperature anomalies were located more towards the west, affecting also Western European countries. This shift is linked to positive SLP and Z500 anomalies situated between the British Isles and Scandinavia.

The most recent 2015 major heat wave (Fig. 4, right column) took place during Aug 3–Aug 15 (13 days), and affected mostly Central and Eastern Europe. Although it was shorter than the 1994 heat wave, extremity indices of both events were comparable, suggesting higher daily temperature anomalies in 2015. The largest positive SLP

anomalies were located north-east of Central Europe, allowing a relatively intense south-easterly advection of tropical air masses.

In addition to the analysis of atmospheric circulation fields, links of the observed major heat waves to precipitation, shortwave radiation, evaporative fraction, and the western and southern flow components and vorticity over Central Europe were analysed (Table 2). All major heat waves were associated with the precipitation deficits during the events and 30 days before their onset. Only roughly one-fifth of precipitation was observed during the major heat waves compared to the 1981–2010 daily based climatology. In the 30-day periods preceding the major heat waves, a reduction of precipitation by approximately 30% was found, with minor differences between the three events. The amount of net solar radiation in ERA-Interim was higher by approximately 20% on average and evaporative fraction was reduced, suggesting a lack of soil moisture, especially during the 2006 and 2015 events.

The average western flow component was reduced while an increase was observed in the southern flow component, indicating enhanced warm south-easterly advection during the major heat waves (both flow component anomalies were

Fig. 4 Sum of positive temperature deviations from the 90% quantile of summer Tmax distribution (*upper row*), mean sea level pressure (*middle row*), and 500 hPa geopotential height (*lower row*) averaged during the 1994 (*left column*), 2006 (*middle column*), and 2015 (*right column*) major heat waves. Anomalies from the summer (JJA) climatology are shown by contour lines
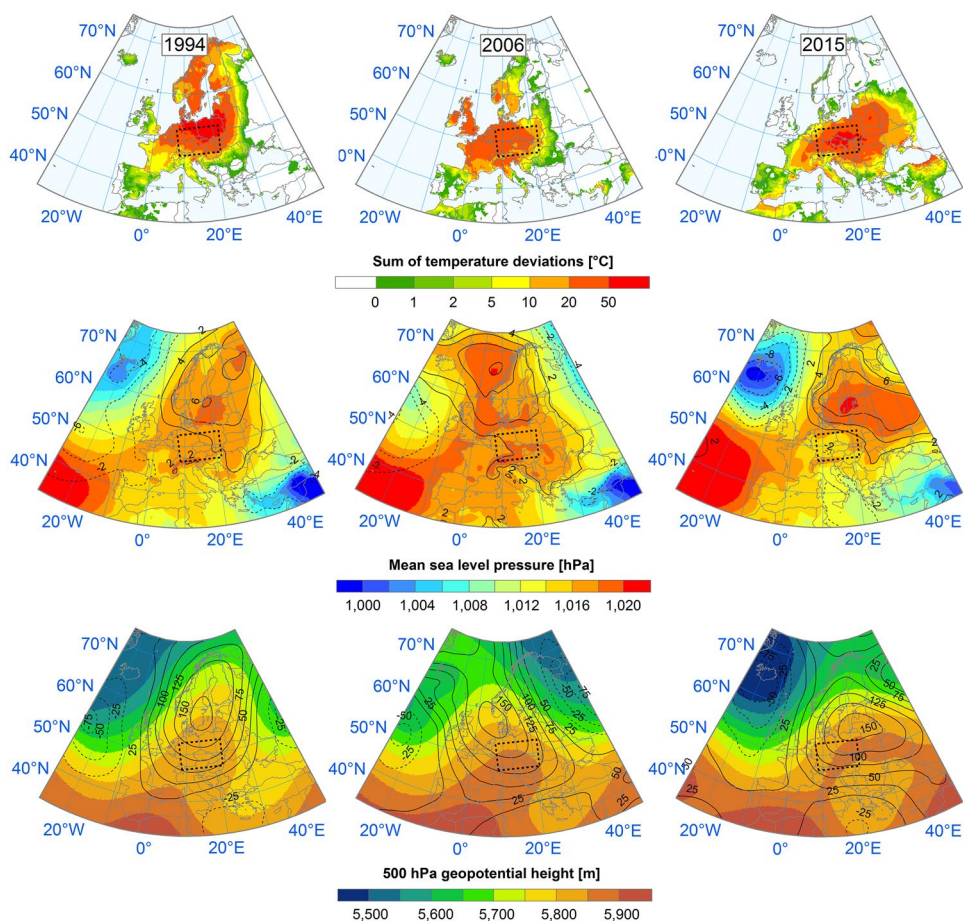
Table 2 Characteristics of major heat waves and associated precipitation, shortwave radiation, evaporative fraction and western and southern flows over Central Europe

Major heat wave	Length (days)	Extremity index (°C)	r (%)	r30 (%)	sw (%)	ef (%)	w (diff)	s (diff)	vort (diff)
1994	16	41.5	18	65	121	94	−1.9	+1.7	+1.8
2006	11	27.1	19	73	122	83	−1.7	+1.6	+1.3
2015	13	39.5	21	70	116	85	−4.5	+2.3	+4.4
mean	13.3	36.0	19.3	69.3	119.7	87.3	−2.7	+1.9	+2.5

r ratio (expressed as a percentage) between precipitation during a heat wave and precipitation climatology (1981–2010) for these days, *r30* ratio (expressed as a percentage) between precipitation during the 30-day period prior to a heat wave and precipitation climatology (1981–2010) for these days, *sw* same as r, but for net shortwave radiation, *ef* same as r, but for evaporative fraction, *w* difference between the western flow component during a heat wave and western flow climatology (1981–2010) for these days, *s* same as w, but for the southern flow component. *vort* same as w, but for vorticity

largest in 2015). Positive anomalies of vorticity were found, which suggests the presence of an SLP field with no distinctive patterns over Central Europe during major heat waves (considering mean negative vorticity in summer, Table 3, final row).

4 EURO-CORDEX RCM simulations

The ensemble mean captured the number of major heat waves and their total extremity index relatively well but large differences were found among individual RCM simulations (Table 3). As described in Sect. 3, observed major heat waves are associated with favourable circulation conditions and lack of available soil moisture for latent cooling. Those RCM simulations that considerably underestimated the total extremity index of major heat waves (or no major heat wave was simulated) failed to reproduce this mechanism. The three lowest values of total extremity index in DMI-HIRHAM-ICHEC, IPSL-WRF-IPSL, and SMHI-RCA-MPI were probably linked to substantially overestimated summertime precipitation (>300 mm, Table 3) and this deficiency was amplified by no soil drying during major heat waves (Table 4). In addition, DMI-HIRHAM-ICHEC simulated an increased zonal flow and IPSL-WRF-IPSL exhibited positive values of vorticity (indicating cyclonic conditions) during major heat waves (Table 4; Fig. 5). However, the mechanisms associated with an underestimation of major heat waves were not fully consistent across all RCM simulations. For example, the total extremity index in CLM-CCLM-MPI (101.6 °C) was close to E-OBS, but its summertime climatology of precipitation, net shortwave radiation, and evaporative fraction suggests rather cold and moist summertime conditions and the model overestimated mean westerly advection (Table 3). These deficiencies are probably compensated by a substantial increment of net shortwave radiation (138%, largest among the RCM simulations)

and the largest increase of southern and decrease of western flow components during major heat waves (Table 4).

By contrast, those RCM simulations that substantially overestimated the total extremity index of major heat waves tended to simulate too-low evaporative fraction and predominant easterly advection during the summer season, which created high potential for the occurrence of major heat waves. The average circulation characteristics were primarily given by driving GCMs. For example, all simulations driven by HadGEM had a negative mean western flow component, while those driven by MPI exhibited quite strong westerly advection in summer (Table 3). Individual RCMs seemed to be capable, however, of modifying the large-scale flow inside their domains.

Although the three highest values of total extremity index were found in the RCA RCM simulations, mechanisms associated with the development of major heat waves were probably different, as discussed below. SMHI-RCA-CNRM and SMHI-RCA-HadGEM suffered from extensive drying during major heat waves (Table 4), resulting in the driest soil conditions among all model simulations (despite too much precipitation during the major heat waves), which probably contributed to the overestimated total magnitude of major heat waves. This behaviour was not observed in SMHI-RCA-IPSL, which simulated soil moisture conditions more realistically.

In addition to the lack of soil moisture during major heat waves, pronounced south-eastern flow and anticyclonic conditions were found in SMHI-RCA-CNRM during these events (Table 4; Fig. 5) and this combination probably resulted in the largest total extremity index (211.8 °C) among all RCM simulations. Favourable circulation conditions were present also in SMHI-RCA-IPSL, which simulated the third largest total extremity index of major heat waves (159.3 °C). By contrast, only minor changes in circulation during major heat waves were found in SMHI-RCA-HadGEM, indicating that soil–atmosphere interactions play an important role in the major heat

Table 3 Evaluation of RCM simulations

RCM simulation	N	D (days)	Ihw (°C)	r JJA (mm)	sw JJA (W*m^{-2})	ef JJA	w JJA	s JJA	vort JJA
CLM-CCLM-CNRM	2	19	58.3	232	185	0.70	−0.2	−2.0	−6.0
CLM-CCLM-HadGEM	5	37	146.3	147	195	0.58	−2.2	−2.3	−2.6
CLM-CCLM-ICHEC	3	23	79.1	245	181	0.74	0.6	−1.7	−6.1
CLM-CCLM-MPI	2	27	101.6	327	159	0.91	3.3	−2.0	−6.4
DMI-HIRHAM-ICHEC	1	12	26.4	306	172	0.87	−0.9	−1.2	−3.4
IPSL-WRF-IPSL	1	12	28.6	307	235	0.72	−3.8	−0.6	0.4
KNMI-RACMO-HadGEM	2	27	115.9	211	186	0.59	−0.1	−0.9	−5.3
KNMI-RACMO-ICHEC	3	32	124.1	248	174	0.65	0.5	−0.8	−4.2
MPI-REMO-MPI	1	14	40.4	255	176	0.83	2.0	−0.6	−6.2
SMHI-RCA-CNRM	4	65	211.8	297	213	0.68	−1.8	−0.5	−2.4
SHMI-RCA-HadGEM	4	50	184.7	218	219	0.64	−1.3	−1.0	−4.4
SHMI-RCA-ICHEC	4	39	126.8	285	208	0.74	0.2	−0.9	−4.0
SHMI-RCA-IPSL	5	49	159.3	284	205	0.75	−0.5	−0.8	−4.6
SHMI-RCA-MPI	0	0	0	315	203	0.78	1.5	−1.0	−5.8
ensemble mean	2.6	29	100.2	263	194	0.70	−0.2	−1.2	−4.4
E-OBS/ERA-Interim	3	40	108.1	244	187	0.72	0.4	−0.7	−5.1

N number of major heat waves in the 1970–2016 period, *D* total duration of major heat waves, *Ihw* total extremity index of major heat waves, *r JJA* summer precipitation climatology (1981–2010), *sw JJA* same as r JJA, but for net shortwave radiation, *ef JJA* same as r JJA, but for evaporative fraction, *w JJA* western flow component climatology (1981–2010), *s JJA* same as w, but for southern flow component, *vort JJA* same as w, but for vorticity

Table 4 Intensity of major heat waves and changes of precipitation, net shortwave radiation, evaporative fraction and atmospheric circulation during major heat waves in the RCM simulations

RCM simulation	Tday (°C)	r HW (%)	r30 HW (%)	sw HW (%)	ef HW (%)	w HW (diff)	s HW (diff)	vort HW (diff)
CLM-CCLM-CNRM	3.1	8	100	122	105	+1.3	+2.5	−8.4
CLM-CCLM-HadGEM	4.0	6	57	119	81	−1.5	+1.9	+8.2
CLM-CCLM-ICHEC	3.4	8	79	128	93	−1.0	+3.2	−1.7
CLM-CCLM-MPI	3.8	27	61	138	86	−4.4	+4.5	−2.9
DMI-HIRHAM-ICHEC	2.2	73	65	120	100	+3.8	+3.2	−7.4
IPSL-WRF-IPSL	2.4	23	86	113	110	−1.8	+3.2	+0.6
KNMI-RACMO-HadGEM	4.3	21	98	128	91	−1.3	+3.4	−1.7
KNMI-RACMO-ICHEC	3.9	21	69	130	90	−1.9	+3.0	+2.5
MPI-REMO-MPI	2.9	30	78	134	85	−3.0	+4.4	−4.4
SMHI-RCA-CNRM	3.3	36	76	114	67	−4.4	+2.6	+1.4
SHMI-RCA-HadGEM	3.7	77	76	108	68	0.0	+0.3	+2.4
SHMI-RCA-ICHEC	3.3	48	70	111	77	−2.8	+3.3	+2.0
SHMI-RCA-IPSL	3.3	53	82	117	94	−2.1	+3.0	+1.7
SHMI-RCA-MPI	–	–	–	–	–	–	–	–
ensemble mean	3.4	33	77	122	88	−1.5	+3.0	−0.6
E-OBS / ERA-Interim	2.7	19	69	119	87	−2.7	+1.9	+2.5

Tday average daily Tmax excesses during major heat waves, *r HW* ratio (expressed as a percentage) between precipitation during a heat wave and precipitation climatology (1981–2010) for these days, *r30 HW* ratio (expressed as a percentage) between precipitation during the 30-day period prior to a heat wave and precipitation climatology (1981–2010) for these days, *sw HW* same as r HW, but for net shortwave radiation, *ef HW* same as r HW, but for evaporative fraction, *w HW* difference between the western flow component during a heat wave and western flow climatology (1981–2010) for these days, *s HW* same as w HW, but for the southern flow component, *vort HW* same as w HW, but for vorticity

Fig. 5 Composite maps of sea level pressure (hPa) during major heat waves in EURO-CORDEX RCMs and ERA-Interim. *N* number of major heat waves, *D* total duration of heat waves (days), *Ihw* total extremity index of heat waves (°C)
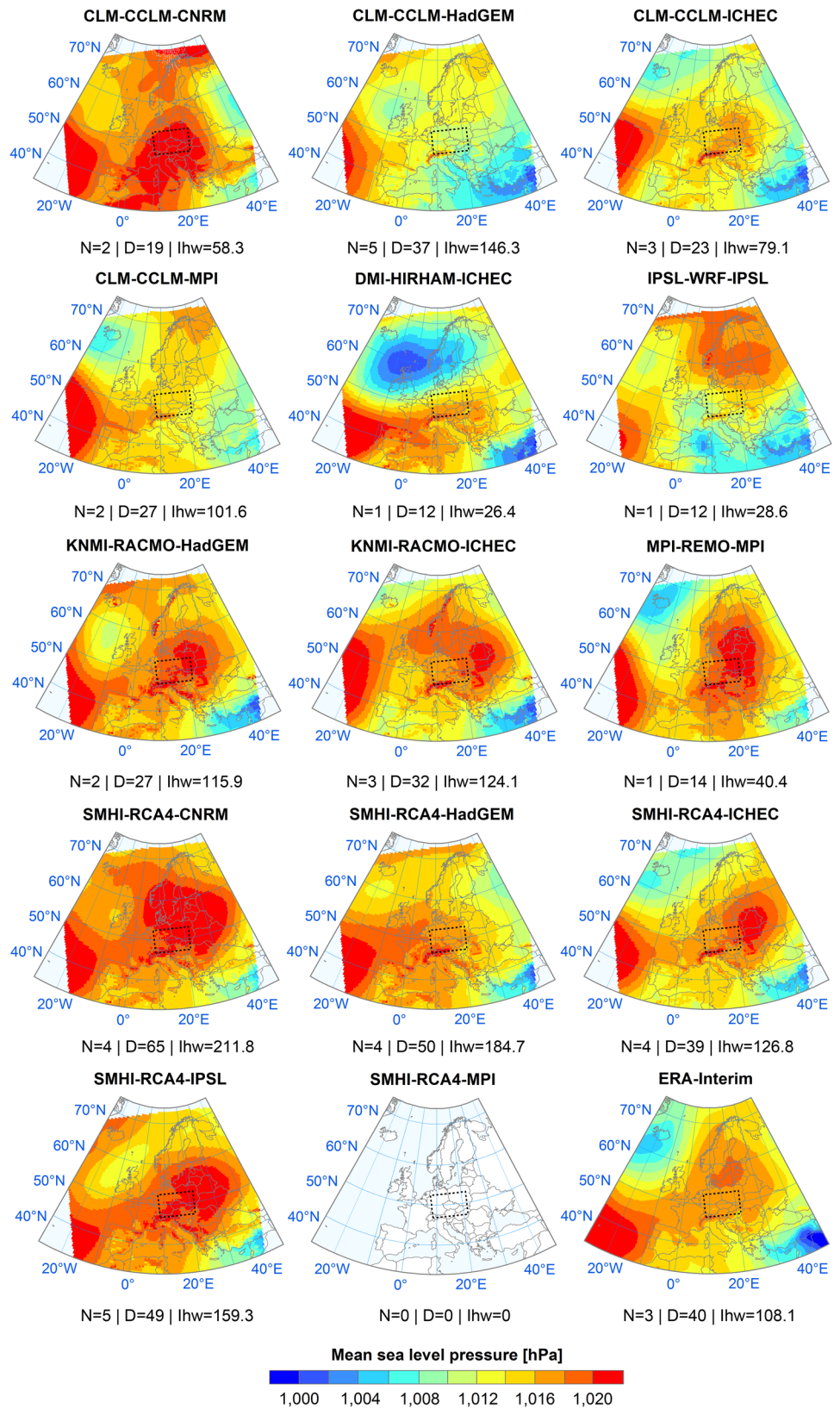
waves' development in this simulation, similarly to CLM-CCLM-HadGEM and to a limited extent KNMI-RACMO-HadGEM. The importance of soil–atmosphere interactions in the RCMs driven by HadGEM possibly originates from the prevailing summertime easterly advection in this GCM, which means that atmospheric circulation is predominantly favourable to high temperature extremes and thus the most extreme major heat waves are mainly triggered by an amplifying effect of the soil moisture deficit.

To sum up, the soil moisture deficit seems to play an important role in the major heat waves' development inasmuch as the five largest values of total extremity index and duration of major heat waves were associated with the substantial decrease of evaporative fraction during these events (except for SMHI-RCA-IPSL, Tables 3, 4). This lack of soil moisture was also quite well linked to amplified average daily Tmax excesses during major heat waves, while moister conditions were associated with relatively low Tmax excesses (Table 4).

Various patterns of SLP and Z500 were simulated during major heat waves by individual RCMs (Figs. 5, 6). In ERA-Interim, major heat waves were related to a high-pressure system situated north of the Central European domain, causing a warm south-easterly advection, with relatively minor differences between the three major heat waves (particularly the two most severe in 1994 and 2015, cf. Fig. 4, middle row). The SLP pattern was associated with Z500 contours with a wavy pattern, exceeding 5,800 m over Central Europe.

This circulation pattern was reproduced with difficulties, because many RCM simulations had a marked anticyclone (in the SLP field) over Europe (> 1,020 hPa), especially RCMs driven by the CNRM GCM. The position of this high-pressure system determined the origin of major heat waves: CLM-CCLM-CNRM simulated these events with rather a radiative nature (strong negative vorticity), while major heat waves in SMHI-RCA-CNRM were rather driven by advective processes (strong eastern and southern flow). These anticyclones were probably not developed throughout the troposphere, because Z500 was not substantially elevated compared to ERA-Interim.

The Z500 pattern associated with major heat waves was reproduced relatively well in the majority of RCMs (Fig. 6). High-amplitude waves in Z500 contours, resembling a developed Ω-blocking pattern, were present in simulations driven by the MPI GCM. This shape of Z500 contours was linked to the overestimated southerly advection during major heat waves that probably compensated too-moist conditions in these simulations. By contrast, waves in Z500 contours in SMHI-RCA-HadGEM had only low amplitude during major heat waves, suggesting a crucial role of soil–atmosphere interaction in this model simulation. DMI-HIRHAM-ICHEC simulated a

pronounced meridional SLP gradient that was linked to anomalous westerly advection during major heat waves (Table 4; Fig. 5), and this pattern was also captured in the Z500 map (Fig. 6).

5 Discussion

5.1 Observed major heat waves and associated meteorological factors

The summer of 2015 was exceptional even at the European scale (Russo et al. 2015), and many stations across Central Europe recorded the highest numbers of very hot days (T$_{max}$ ≥35 °C, Hoy et al. 2016). The summer was anomalous also from the hydrological perspective; Orth et al. (2016) reported that it was even drier in Central Europe than the well-known 2003 and 2010 summers, according to cumulative precipitation. The previous 1994 and 2006 major heat waves were the most distinctive since the beginning of temperature measurements in Central Europe (1775 in Prague, according to the sum of Tmax excesses above 30 °C; Kyselý 2010). Together with the 2015 major heat wave this clearly illustrates that recent decades have been exceptional as to summer temperature conditions in Central Europe over the whole period of observed records.

Although Central European heat waves are associated with several circulation patterns (e.g. Kyselý 2008; Tomczyk and Bednorz 2016), all major heat waves analysed in the present study are linked to a similar pattern dominated by positive anomalies of SLP and Z500 centred north to northeast from the Central European domain. This circulation pattern may be preferred for major heat waves' development due to its persistence, and it is probably related to the so-called Scandinavian blocking, associated with Rossby waves' breaking events (Michel et al. 2012). In accordance with previous studies (Fischer et al. 2007; Stéfanon et al. 2014), all observed major heat waves were preceded by a precipitation deficit that amplifies Tmax through a reduced cooling effect of latent heat.

Duchez et al. (2016) hypothesised that a North Atlantic cold ocean anomaly in 2015 and the resulting strong meridional sea surface temperature gradient could have triggered a propagating Rossby wave train, causing a stationary jet stream position that favoured the development of positive 850 hPa geopotential height anomaly and temperature extremes over Central Europe during the summer of 2015. A heat wave's life cycle seems to be more complex, however, since Plavcová and Kyselý (2016) showed that anticyclonic circulation types (with dominant radiative heating due to clear-sky conditions) prevail before the onset of heat waves while southerly and easterly types (in which warm advection plays a more important role)

Fig. 6 Composite maps of 500 hPa geopotential height (m) during major heat waves in EURO-CORDEX RCMs and ERA-Interim. *N* number of major heat waves, *D* total duration of heat waves (days), *Ihw* total extremity index of heat waves (°C)
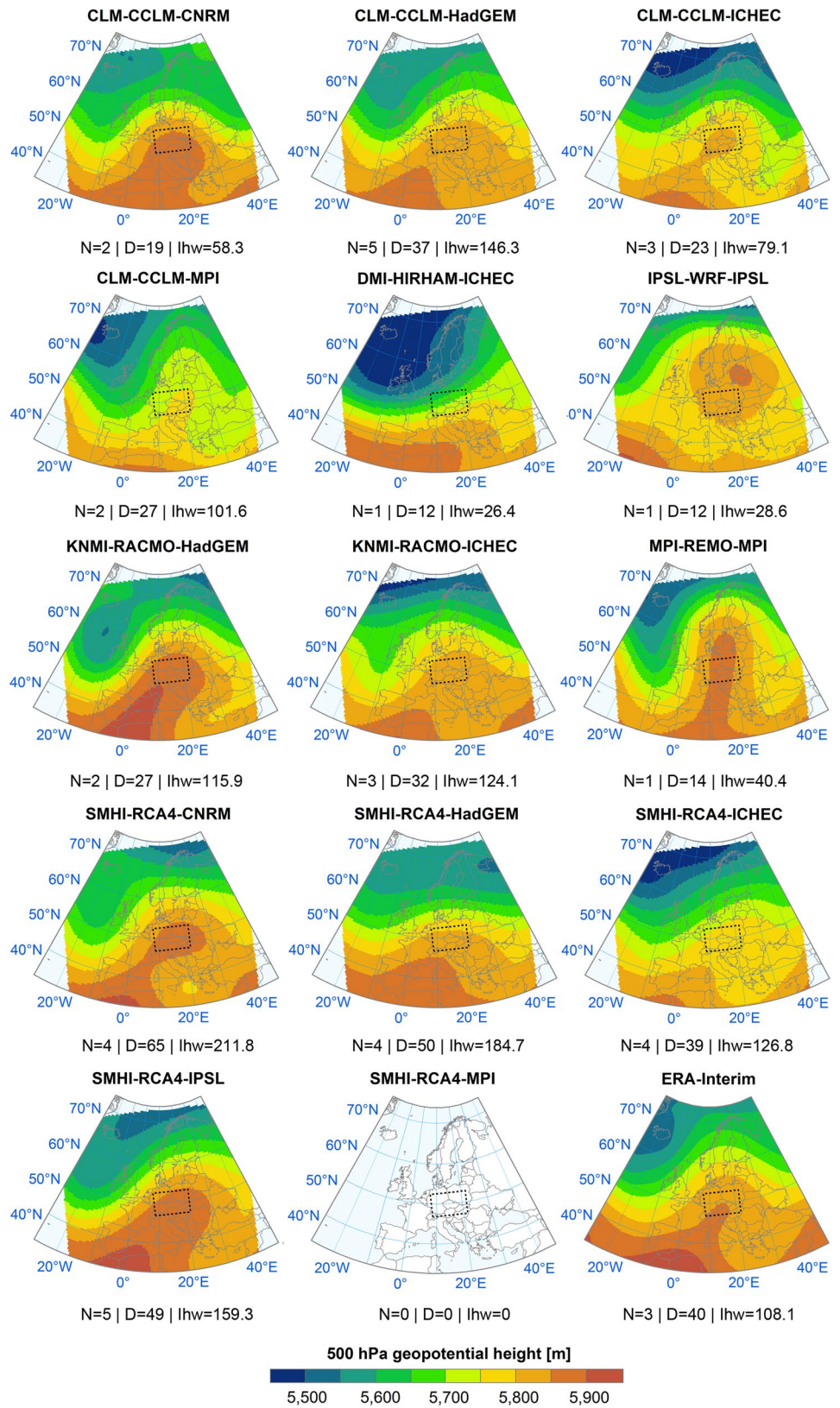
become dominant during heat waves and support their development and persistence.

5.2 Simulated major heat waves and their associated meteorological factors

The joint effect of favourable and persistent circulation and reduced soil-moisture, which is important for the development of major heat waves, was simulated with difficulties. Some RCMs tended to establish a soil moisture-limited regime across Central Europe. This behaviour was reported by Stegehuis et al. (2013) using a previous generation of ENSEMBLES RCMs driven by reanalysis, indicating that this deficiency was not fully solved. The inconsistency is probably linked mainly to biases in the simulation of convective precipitation and surface fluxes in RCMs that use parameterizations and do not resolve these processes explicitly (Jin et al. 2010; Rauscher et al. 2010).

Moreover, this deficiency probably originated not only from the RCMs, because a lack of soil moisture was present especially in those RCMs driven by the HadGEM GCM in our study. The reduced evaporative fraction in SMHI-RCA-HadGEM was surprisingly associated with the largest precipitation during major heat waves among all RCM simulations. Although we do not have a clear explanation for this behaviour, the discrepancy may originate from joint effects of (i) a tendency of the RCA RCM to overestimate precipitation during severe heat waves (Lhotka and Kyselý 2015b), and (ii) the prevailing summertime easterly advection along with low precipitation in simulations driven by the HadGEM GCM (Sect. 4). These contradictory factors may create nonstandard interactions between convective and land-surface schemes in this RCM simulation.

Despite the fact that the Tmax excesses were overestimated, the mean magnitude of major heat waves was comparable to observed data. This is related to an underestimated mean number and duration of major heat waves in the RCM simulations, which is in contrast with Vautard et al. (2013) and Plavcová and Kyselý (2016), who concluded that RCMs tended to simulate too-persistent heat waves. These seemingly contrasting results are probably associated with different definitions of events. In our study, we analysed only major heat waves that lasted for roughly two weeks. They probably were related to atmospheric blocking events that are reported to be underestimated in climate models (Scaife et al. 2010), which may be associated with the underestimated duration and frequency of major heat waves in RCM simulations.

5.3 Possible limitations of major heat waves' analysis

As the study deals with major heat waves, the results need to be discussed with caution due to a relatively small number of events (given the length of observed records and RCM simulations). Only three major heat waves occurred since 1950 in the observed data. The sample size would be larger (in observed as well as RCM-simulated data) with a lower threshold used to delimit events that are considered "major", but this would draw the analysis from the focus on extreme heat waves (that deserve attention also because the society's vulnerability to their impacts, which is much larger than in case of ordinary heat waves, Kharin et al. 2007). Similar limitations were encountered by Beniston (2004), who studied modelled events analogous to the 2003 heat wave in Western Europe, and by Barriopedro et al. (2011), who dealt with the 2003 and 2010 heat waves in RCMs.

In addition, main features of SLP and Z500 patterns may be faded in the composite maps due to an averaging of individual major heat waves, especially in those RCM simulations in which land–atmosphere interaction plays a vital role for the development of major heat waves. For example, three of five major heat waves in CLM-CCLM-HadGEM were associated with an enhanced eastern flow, while the other two were linked to westerly advection (not shown). This may contribute to the indistinct SLP field in the composite map in this RCM simulation.

6 Conclusions

Major Central European heat waves in an ensemble of EURO-CORDEX RCM simulations driven by GCMs were analysed. We evaluated their severity and associated meteorological factors against the observed major heat waves (1994, 2006, and 2015) using the E-OBS data set and the ERA-Interim reanalysis. The key findings can be summarized as follows:

- The summer of 2015 was the most pronounced in Central Europe since 1950 according to the seasonal sum of the heat waves' extremity index. The most severe heat wave during this summer persisted for 13 days between Aug 3 and Aug 15 and along with the 1994 and 2006 events, it represents one of the three major heat waves that are characterized by long duration and high extremity index. These events are probably exceptional in the context of observed records in Central Europe since 1775.
- These major heat waves were related to circulation patterns resembling Ω-shaped blocking, which is characterized by reduced zonal flow, allowing meridional advection of warm air masses. Precipitation deficits were also observed during and before heat waves along with reduced evaporative fraction and increased net shortwave radiation.
- The value of the total extremity index of major heat waves in the ensemble mean was close to observed data, but substantial differences were present in individual

RCM simulations. These variations were linked to the representation of large-scale circulation and land–atmosphere interactions. Overestimation of the number and duration of major heat waves in some RCMs was related to a combination of strong south-easterly advection and depletion of soil moisture, while their underestimation was mainly associated with too-moist summertime conditions.

- In some RCM simulations, the seemingly good reproduction of the total extremity index of major heat waves was erroneously achieved through unfavourable circulation conditions compensated by a substantial lack of available soil moisture and vice versa. Although these mechanisms seem to be physically realistic, no analogous situation was found in the observed data since the mid-twentieth century.

The last point emphasizes the importance of evaluating not only resulting climatological characteristics, but also their associated meteorological factors. It should be noted that successful representation of major heat waves' driving mechanisms in historical climate does not guarantee a credible simulation of these events in the future climate, but it does provide some guidance for the selection of a suitable ensemble of RCM simulations for further analyses. Although the design of an objective performance metric for RCM simulations is beyond the scope of this article, the CCLM, RACMO, and RCA RCMs driven by the ICHEC-EC-EARTH GCM performed best in simulating the total magnitude of Central European major heat waves and their links to meteorological factors. In other words, the characteristics of major heat waves in these model simulations were most similar to what we observe in the real world.

References

Baldocchi D, Falge E, Gu L et al (2001) FLUXNET: A New Tool to Study the Temporal and Spatial Variability of Ecosystem-Scale Carbon Dioxide, Water Vapor, and Energy Flux Densities. Bull Am Meteorol Soc 82:2415–2434. doi:10.1175/1520-0477(2001)082<2415:FANTTS>2.3.CO;2

Ballester J, Rodó X, Giorgi F (2010) Future changes in Central Europe heat waves expected to mostly follow summer mean warming. Clim Dyn 35:1191–1205. doi:10.1007/s00382-009-0641-5

Barriopedro D, Fischer EM, Luterbacher J et al (2011) The hot summer of 2010: redrawing the temperature record map of Europe. Science 332:220–224. doi:10.1126/science.1201224

Bastos A, Gouveia CM, Trigo RM, Running SW (2014) Analysing the spatio-temporal impacts of the 2003 and 2010 extreme heatwaves on plant productivity in Europe. Biogeosciences 11:3421–3435. doi:10.5194/bg-11-3421-2014

Beniston M (2004) The 2003 heat wave in Europe: A shape of things to come? An analysis based on Swiss climatological data and model simulations. Geophys Res Lett 31:4. doi:10.1029/2003GL018857

Berg A, Lintner B, Findell K et al (2014) Impact of soil moisture–atmosphere interactions on surface temperature distribution. J Clim 27:7976–7993. doi:10.1175/JCLI-D-13-00591.1

Blenkinsop S, Jones PD, Dorling SR, Osborn TJ (2009) Observed and modelled influence of atmospheric circulation on central England temperature extremes. Int J Climatol 29:1642–1660. doi:10.1002/joc.1807

Davin EL, Maisonnave E, Seneviratne SI (2016) Is land surface processes representation a possible weak link in current Regional Climate Models? Environ Res Lett 11:74027. doi:10.1088/1748-9326/11/7/074027

De Bono A, Giuliani G, Kluser S, Peduzzi P (2004) Impacts of summer 2003 heat wave in Europe. UNEP/DEWA/GRID-Europe Environ Alert Bull 2:1–4

Dee DP, Uppala SM, Simmons AJ et al (2011) The ERA-Interim reanalysis: configuration and performance of the data assimilation system. Q J R Meteorol Soc 137:553–597. doi:10.1002/qj.828

Della-Marta PM, Luterbacher J, Weissenfluh H et al (2007) Summer heat waves over western Europe 1880–2003, their relationship to large-scale forcings and predictability. Clim Dyn 29:251–275. doi:10.1007/s00382-007-0233-1

Duchez A, Frajka-Williams E, Josey SA et al (2016) Drivers of exceptionally cold North Atlantic Ocean temperatures and their link to the 2015 European heat wave. Environ Res Lett 11:74004. doi:10.1088/1748-9326/11/7/074004

Fischer EM (2014) Climate science: Autopsy of two mega-heatwaves. Nat Geosci 7:332–333. doi:10.1038/ngeo2148

Fischer EM, Schär C (2010) Consistent geographical patterns of changes in high-impact European heatwaves. Nat Geosci 3:398–403. doi:10.1038/ngeo866

Fischer EM, Seneviratne SI, Lüthi D, Schär C (2007) Contribution of land-atmosphere coupling to recent European summer heat waves. Geophys Res Lett 34:L06707. doi:10.1029/2006GL029068

Haarsma RJ, Selten F, van den Hurk B et al (2009) Drier Mediterranean soils due to greenhouse warming bring easterly winds over summertime central Europe. Geophys Res Lett 36:L04705. doi:10.1029/2008GL036617

Haylock MR, Hofstra N, Klein Tank AMG et al (2008) A European daily high-resolution gridded data set of surface temperature and precipitation for 1950–2006. J Geophys Res 113:D20119. doi:10.1029/2008JD010201

Hoy A, Hänsel S, Skalak P et al (2016) The extreme European summer of 2015 in a long-term perspective. Int J Climatol. doi:10.1002/joc.4751

Jacob D, Petersen J, Eggert B et al (2014) EURO-CORDEX: new high-resolution climate change projections for European impact research. Reg Environ Chang 14:563–578. doi:10.1007/s10113-013-0499-2

Jaeger EB, Seneviratne SI (2011) Impact of soil moisture–atmosphere coupling on European climate extremes and trends in a regional climate model. Clim Dyn 36:1919–1939. doi:10.1007/s00382-010-0780-8

Jenkinson AF, Collison FP (1977) An initial climatology of gales over the North Sea. Meteorological Office, Bracknell, Synoptic Climatology Branch Memorandum No. 62

Jin J, Miller NL, Schlegel N (2010) Sensitivity Study of Four Land Surface Schemes in the WRF Model. Adv Meteorol 2010:1–11. doi:10.1155/2010/167436

Kharin VV, Zwiers FW, Zhang X, Hegerl GC (2007) Changes in temperature and precipitation extremes in the IPCC ensemble of global coupled model simulations. J Clim 20:1419–1444. doi:10.1175/JCLI4066.1

Kirtman B, Power SB, Adedoyin JA et al (2013) Near-term Climate Change: Projections and Predictability. In: Climate Change 2013: The Physical Science Basis. Cambridge University Press, Cambridge

Konovalov IB, Beekmann M, Kuznetsova IN et al (2011) Atmospheric impacts of the 2010 Russian wildfires: Integrating modelling and measurements of an extreme air pollution episode in the Moscow region. Atmos Chem Phys 11:10031–10056. doi:10.5194/acp-11-10031-2011

Kotlarski S, Keuler K, Christensen OB et al (2014) Regional climate modeling on European scales: A joint standard evaluation of the EURO-CORDEX RCM ensemble. Geosci Model Dev 7:1297–1333. doi:10.5194/gmd-7-1297-2014

Kyselý J (2008) Influence of the persistence of circulation patterns on warm and cold temperature anomalies in Europe: Analysis over the 20th century. Glob Planet Change 62:147–163. doi:10.1016/j.gloplacha.2008.01.003

Kyselý J (2010) Recent severe heat waves in central Europe: how to view them in a long-term prospect? Int J Climatol 109:89–109. doi:10.1002/joc1874

Lau NC, Nath MJ (2014) Model simulation and projection of European heat waves in present-day and future climates. J Clim 27:3713–3730. doi:10.1175/JCLI-D-13-00284.1

Lhotka O, Kyselý J (2015a) Characterizing joint effects of spatial extent, temperature magnitude and duration of heat waves and cold spells over Central Europe. Int J Climatol 35:1232–1244. doi:10.1002/joc.4050

Lhotka O, Kyselý J (2015b) Spatial and temporal characteristics of heat waves over Central Europe in an ensemble of regional climate model simulations. Clim Dyn 45:2351–2366. doi:10.1007/s00382-015-2475-7

Lhotka O, Kyselý J, Farda A (2017) Climate change scenarios of heat waves in Central Europe and their uncertainties. Theor Appl Climatol. doi:10.1007/s00704-016-2031-3

Michel C, Rivière G, Terray L, Joly B (2012) The dynamical link between surface cyclones, upper-tropospheric Rossby wave breaking and the life cycle of the Scandinavian blocking. Geophys Res Lett 39:6. doi:10.1029/2012GL051682

Orth R, Zscheischler J, Seneviratne SI (2016) Record dry summer in 2015 challenges precipitation projections in Central Europe. Sci Rep 6:28334. doi:10.1038/srep28334

Plavcová E, Kyselý J (2012) Atmospheric circulation in regional climate models over Central Europe: links to surface air temperature and the influence of driving data. Clim Dyn 39:1681–1695. doi:10.1007/s00382-011-1278-8

Plavcová E, Kyselý J (2016) Overly persistent circulation in climate models contributes to overestimated frequency and duration of heat waves and cold spells. Clim Dyn 46:2805–2820. doi:10.1007/s00382-015-2733-8

Rauscher SA, Coppola E, Piani C, Giorgi F (2010) Resolution effects on regional climate model simulations of seasonal precipitation over Europe. Clim Dyn 35:685–711. doi:10.1007/s00382-009-0607-7

Robine J-M, Cheung SLK, Le Roy S et al (2008) Death toll exceeded 70,000 in Europe during the summer of 2003. C R Biol 331:171–178. doi:10.1016/j.crvi.2007.12.001

Russo S, Sillmann J, Fischer EM (2015) Top ten European heatwaves since 1950 and their occurrence in the future. Environ Res Lett 10:124003. doi:10.1088/1748-9326/10/12/124003

Scaife AA, Woollings T, Knight J et al (2010) Atmospheric Blocking and Mean Biases in Climate Models. J Clim 23:6143–6152. doi:10.1175/2010JCLI3728.1

Schubert SD, Wang H, Koster R et al (2014) Northern Eurasian heat waves and droughts. J Clim 27:3169–3207. doi:10.1175/JCLI-D-13-00360.1

Shaposhnikov D, Revich B, Bellander T et al (2014) Mortality related to air pollution with the moscow heat wave and wildfire of 2010. Epidemiology 25:359–364. doi:10.1097/EDE.0000000000000090

Stéfanon M, Drobinski P, D'Andrea F et al (2014) Soil moisture-temperature feedbacks at meso-scale during summer heat waves over Western Europe. Clim Dyn 42:1309–1324. doi:10.1007/s00382-013-1794-9

Stegehuis AI, Vautard R, Ciais P et al (2013) Summer temperatures in Europe and land heat fluxes in observation-based data and regional climate model simulations. Clim Dyn 41:455–477. doi:10.1007/s00382-012-1559-x

Thomson AM, Calvin KV, Smith SJ et al (2011) RCP4.5: A pathway for stabilization of radiative forcing by 2100. Clim Change 109:77–94. doi:10.1007/s10584-011-0151-4

Tomczyk AM, Bednorz E (2016) Heat waves in Central Europe and their circulation conditions. Int J Climatol 36:770–782. doi:10.1002/joc.4381

van der Linden P, Mitchell JFB (2009) ENSEMBLES: climate change and its impacts: summary of research and results from the ENSEMBLES project. Met Office Hadley Centre, Exeter

Vautard R, Gobiet A, Jacob D et al (2013) The simulation of European heat waves from an ensemble of regional climate models within the EURO-CORDEX project. Clim Dyn 41:2555–2575. doi:10.1007/s00382-013-1714-z